Photon pair production with soft gluon resummation in hadronic interactions

C. Balázs,[1] E. L. Berger,[2] S. Mrenna,[2] and C.-P. Yuan[1]
[1]*Department of Physics and Astronomy, Michigan State University, East Lansing, Michigan 48824*
[2]*High Energy Physics Division, Argonne National Laboratory, Argonne, Illinois 60439*
(Received 26 January 1998; published 12 May 1998)

The production rate and kinematic distributions of isolated photon pairs produced in hadron interactions are studied. The effects of the initial-state multiple soft-gluon emission to the scattering subprocesses $q\bar{q}, qg$, and $gg \to \gamma\gamma X$ are resummed with the Collins-Soper-Sterman soft gluon resummation formalism. The effects of fragmentation photons from $qg \to \gamma q$, followed by $q \to \gamma X$, are also studied. The results are compared with data from the Fermilab Tevatron collider. A prediction of the production rate and kinematic distributions of the diphoton pair in proton-nucleon reactions is also presented.
[S0556-2821(98)05111-X]

PACS number(s): 13.85.Qk, 12.38.Cy

I. INTRODUCTION

An increasing amount of prompt diphoton data is becoming available from the Tevatron collider and the fixed-target experiments at Fermilab. A comparison of the data to the calculation of the diphoton production rate and kinematic distributions provides a test of many aspects of perturbative quantum chromodynamics (PQCD). Furthermore, understanding the diphoton data is important for new physics searches. For example, diphoton production is an irreducible background to the light Higgs boson decay mode $h \to \gamma\gamma$. The next-to-leading order (NLO) cross section for the $p\bar{p} \to \gamma\gamma X$ process [1] was shown to describe well the invariant mass distribution of the diphoton pair after the leading order (LO) $gg \to \gamma\gamma$ contribution (from one-loop box diagrams) was included [2,3]. However, to accurately describe the distribution of the transverse momentum of the photon pair and the kinematical correlation of the two photons, a calculation has to be performed that includes the effects of initial-state multiple soft-gluon emission. In hard scattering processes, the dynamics of the multiple soft-gluon radiation is predicted by resummed PQCD [4–13].

In this work, the Collins-Soper-Sterman (CSS) soft gluon resummation formalism, developed for Drell-Yan pair (including W and Z boson) production [7], is extended to describe the production of photon pairs. This extension is similar to the formalism developed for describing the distribution of the leptons from vector boson decays [10] because the final state of the diphoton process is also a color singlet state at LO. Initial-state multiple soft-gluon emission in the scattering subprocesses $q\bar{q}, qg$ and $gg \to \gamma\gamma X$ is resummed by treating the photon pair $\gamma\gamma$ similarly to the Drell-Yan photon γ^*. In addition, there are contributions in which one of the final photons is produced through a long-distance fragmentation process. An example is $qg \to \gamma q$ followed by the fragmentation of the final state quark $q \to \gamma X$. An earlier study of soft-gluon resummation effects in photon pair production may be found in Ref. [14].

The results of this overall calculation are compared with Collider Detector at Fermilab (CDF) [15] and DØ [16] data taken at the collider energy $\sqrt{S} = 1.8$ TeV. A prediction for the production rate and kinematic distributions of the diphoton pair in proton-nucleon interactions at the fixed-target energy $\sqrt{S} = 31.5$ GeV, appropriate for the E706 experiment at Fermilab [17], is also presented.

Section II reviews some properties of the fixed order calculation of the production rate and kinematics of photon pairs. Section III presents the soft gluon resummation formalism and its application to diphoton production. The numerical results of this study, and a comparison with data, are presented in Sec. IV. Finally, Sec. V contains a discussion of the results and conclusions.

II. DIPHOTON PRODUCTION AT LEADING AND NEXT-TO-LEADING ORDER

The leading order subprocesses for diphoton production in hadron interactions are of order α_{em}^2, where α_{em} denotes the electromagnetic coupling strength. There are three classes of LO partonic contributions to the reaction $h_1 h_2 \to \gamma\gamma X$, where h_1 and h_2 are hadrons, illustrated in Figs. 1(a)–1(c). The first [Fig. 1(a)] is the short-distance $q\bar{q} \to \gamma\gamma$ subprocess. The second [Fig. 1(b)] is the convolution of the short-distance $qg \to \gamma q$ subprocess with the long-distance fragmentation of the final state quark $q \to \gamma X$. This is a LO contribution since the hard scattering is of order $\alpha_{em}\alpha_s$, while fragmentation is effectively of order α_{em}/α_s. Here, α_s denotes the QCD coupling strength. Class 1(b) also includes the subprocess $q\bar{q} \to \gamma g$ convoluted with the fragmentation $g \to \gamma X$. Finally, there are LO contributions [Fig. 1(c)] involving subprocesses like $qq \to qq$, where both final state quarks fragment $q \to \gamma X$. The transverse momenta of the photons are denoted $\vec{p}_{T_1}$ and $\vec{p}_{T_2}$, and the transverse momentum of the pair is $\vec{Q}_T = \vec{p}_{T_1} + \vec{p}_{T_2}$. In the absence of transverse momentum carried by the incident partons, the LO process 1(a) provides $\vec{Q}_T = 0$. With the added assumption of collinear final-state fragmentation, Fig. 1(b) provides $\vec{Q}_T = \vec{p}_{T_1} + \vec{p}_{T_2} = (1-z)\vec{p}_{T_1}$, where photon 2 carries a fraction z of the momentum of the final-state quark. Given a lower limit on the magnitude of the transverse momentum p_T^γ of

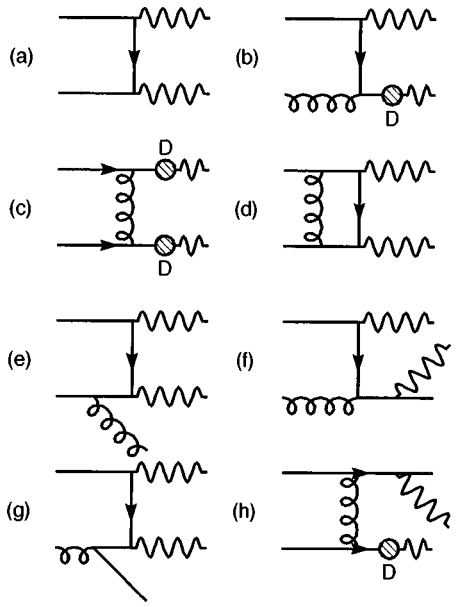

FIG. 1. Feynman diagrams representing the leading order and next-to-leading order contributions to photon pair production in hadron collisions. The shaded circles signify the production of long-distance fragmentation photons, which are described by the fragmentation function $D_{\gamma\leftarrow q}$.

each photon, the total cross section at LO is finite.

The next-to-leading order subprocesses for diphoton production are of order $\alpha_{em}^2\alpha_s$. One class of one-loop Feynman diagrams [Fig. 1(d)] contributes by interfering with the tree level diagram 1(a). Real gluon emission [Fig. 1(e)] is also present at NLO. The subprocess $qg\rightarrow\gamma\gamma q$ contains a singular piece [Fig. 1(f)] that renormalizes the lower order fragmentation [Fig. 1(b)] and a piece [Fig. 1(g)] that is free of final-state collinear singularities. Finally, subprocesses like $qq\rightarrow qq\gamma\gamma$ contain a regular piece involving photon emission convoluted with a fragmentation function [Fig. 1(h)] and pieces that renormalize the double fragmentation process [Fig. 1(c)]. The regular 3-body final state contributions from Figs. 1(e), 1(f), and 1(g) provide $\vec{Q}_T=-\vec{p}_{T_j}$, where j represents the final-state quark or gluon. The full set of NLO contributions just described is free of final-state singularities, and the total integrated cross section at NLO is finite for a finite lower limit on each p_T^γ.

Higher order calculations in α_s improve the accuracy of predictions for total cross sections involving quarks or gluons when only one hard scale Q is relevant. For $h_1h_2\rightarrow\gamma\gamma X$, this scale can be chosen proportional to the invariant mass of the photon pair, $Q=M_{\gamma\gamma}$, which is about equal to $2p_T^\gamma$ for two well-separated photons in the central rapidity region. For kinematic distributions that depend on more than one scale, a NLO calculation may be less reliable. One example is the distribution of the transverse momentum of the photon pair, $Q_T=|\vec{Q}_T|$. At fixed Q, the behavior for small Q_T of the NLO contribution to the differential cross section has the form

$$\frac{d\sigma}{dQ_T^2}=\sigma_0\frac{\alpha_s}{\pi}\frac{1}{Q_T^2}\left[a_1\ln\left(\frac{Q^2}{Q_T^2}\right)+a_0\right], \tag{1}$$

where a_0 and a_1 are dimensionless constants, and $\sigma_0(Q)$ is the total LO cross section calculated from the subprocess 1(a). The structure of Eq. (1) indicates that the fixed order QCD prediction is reliable when $Q_T\simeq Q$, but becomes less reliable when $Q_T\ll Q$, where $\ln(Q^2/Q_T^2)$ becomes large. In the region $Q_T\ll Q$, the photon pair is accompanied by soft and/or collinear gluon radiation. To calculate distributions like $d\sigma/dQ_T^2$ reliably in the region $Q_T\ll Q$, effects of multiple soft gluon emission must be taken into account explicitly [4–13]. The contributions 1(e) and 1(g) exhibit singular behavior that can be tamed by resummation of the effects of initial-state multiple soft-gluon radiation to all orders in α_s. Other contributions that do not become singular as $Q_T\rightarrow 0$ do not need to be treated in this manner. Fragmentation contributions like Fig. 1(b) are found to be small in magnitude after isolation restrictions are imposed on the energy of the hadronic remnant from the fragmentation. Therefore, contributions like Figs. 1(c) and 1(h) are ignored in this work. Gluon fragmentation to a photon can be ignored, since its magnitude is small.

The subprocess $gg\rightarrow\gamma\gamma$, involving a quark box diagram, is of order $\alpha_{em}^2\alpha_s^2$. While formally of even higher order than the NLO contributions considered so far, this LO gg contribution is enhanced by the size of the gluon parton distribution function. Consideration of the order $\alpha_{em}^2\alpha_s^3$ correction leads to resummation of the gg subprocess in a manner analogous to the $q\bar{q}$ resummation.

III. SOFT GLUON RESUMMATION FORMALISM

To improve upon the prediction of Eq. (1) for the region $Q_T\ll Q$, perturbation theory can be applied using an expansion parameter $\alpha_s^m\ln^n(Q^2/Q_T^2)$, with $n=0,\ldots,2m-1$, instead of α_s^m. The terms $\alpha_s^m\ln^n(Q^2/Q_T^2)$ represent the effects of soft gluon emission at order α_s^m. Resummation of the singular part of the perturbative series to all orders in α_s by Sudakov exponentiation yields a regular differential cross section as $Q_T\rightarrow 0$.

The differential cross section in the CSS resummation formalism for the production of photon pairs in hadron collisions can be written as an integral in impact parameter b space:

$$\begin{aligned}\frac{d\sigma(h_1h_2\rightarrow\gamma_1\gamma_2X)}{dQ^2dy\,dQ_T^2d\cos\theta d\phi}&=\frac{1}{24\pi S}\frac{1}{Q^2}\left\{\frac{1}{(2\pi)^2}\int d^2b e^{i\vec{Q}_T\cdot\vec{b}}\right.\\&\times\sum_{i,j}\widetilde{W}_{ij}(b_*,Q,x_1,x_2,\theta,\phi,C_1,C_2,C_3)\\&\left.\times\widetilde{W}_{ij}^{NP}(b,Q,x_1,x_2)+Y(Q_T,Q,x_1,x_2,\theta,\phi,C_4)\right\}.\end{aligned} \tag{2}$$

The variables Q, y, and Q_T are the invariant mass, rapidity, and transverse momentum of the photon pair in the laboratory frame, while θ and ϕ are the polar and azimuthal angles

of one of the photons in the Collins-Soper frame [18]. The initial-state parton momentum fractions are defined as $x_1 = e^y Q/\sqrt{S}$, and $x_2 = e^{-y} Q/\sqrt{S}$, and $\sqrt{S}$ is the center-of-mass (c.m.) energy of the hadrons h_1 and h_2.

The renormalization group invariant quantity $\widetilde{W}_{ij}(b)$ sums the large logarithmic terms $\alpha_s^m \ln^n(b^2Q^2)$ to all orders in α_s. For a hard scattering process initiated by the partons i and j,

$$\begin{aligned}\widetilde{W}_{ij}(b,Q,x_1,x_2,\theta,\phi,C_1,C_2,C_3) &= \exp\{-\mathcal{S}_{ij}(b,Q,C_1,C_2)\}[\mathcal{C}_{i/h_1}(x_1)\mathcal{C}_{j/h_2}(x_2) \\ &\quad + \mathcal{C}_{j/h_1}(x_1)\mathcal{C}_{i/h_2}(x_2)]\mathcal{F}_{ij}(\alpha_{em}(C_2Q),\alpha_s(C_2Q),\theta,\phi),\end{aligned} \tag{3}$$

where $\mathcal{F}_{ij}$ is a kinematic factor that depends also on the coupling constants, and $\mathcal{C}_{i/h}(x)$ denotes the convolution of the parton distribution function (PDF) $f_{a/h}$ (for parton a inside hadron h) with the perturbative Wilson coefficient functions $C_{ij}^{(n)}$:

$$\mathcal{C}_{i/h_1}(x_1) = \sum_a \int_{x_1}^1 \frac{d\xi_1}{\xi_1} C_{ia}^{(n)}\left(\frac{x_1}{\xi_1}, b, \mu = \frac{C_3}{b}, C_1, C_2\right) \times f_{a/h_1}\left(\xi_1, \mu = \frac{C_3}{b}\right). \tag{4}$$

The Sudakov exponent $\mathcal{S}_{ij}(b,Q,C_1,C_2)$ in Eq. (3) is defined as

$$\mathcal{S}_{ij}(b,Q,C_1,C_2) = \int_{C_1^2/b^2}^{C_2^2Q^2} \frac{d\bar{\mu}^2}{\bar{\mu}^2}\left[A_{ij}(\alpha_s(\bar{\mu}),C_1)\ln\left(\frac{C_2^2Q^2}{\bar{\mu}^2}\right) + B_{ij}(\alpha_s(\bar{\mu}),C_1,C_2)\right]. \tag{5}$$

The coefficients A_{ij} and B_{ij} and the functions C_{ij} can be calculated perturbatively in powers of α_s/π, so that $A_{ij} = \Sigma_{n=1}^{\infty}(\alpha_s/\pi)^n A_{ij}^{(n)}$, $B_{ij} = \Sigma_{n=1}^{\infty}(\alpha_s/\pi)^n B_{ij}^{(n)}$, and $C_{ij} = \Sigma_{n=0}^{\infty}(\alpha_s/\pi)^n C_{ij}^{(n)}$.

The dimensionless constants C_1, C_2 and $C_3 \equiv \mu b$ were introduced in the solution of the renormalization group equations for $\widetilde{W}_{ij}$. The constant C_1 determines the onset of nonperturbative physics, C_2 specifies the scale of the hard scattering process, and $\mu = C_3/b$ is the factorization scale at which the $C_{ij}^{(n)}$ functions are evaluated. A conventional choice of the renormalization constants is $C_1 = C_3 = 2e^{-\gamma_E} \equiv b_0$ and $C_2 = C_4 = 1$ [7], where γ_E is the Euler constant. These choices of the renormalization constants are used in the numerical results of this work because they eliminate large constant factors (depending on C_1, C_2 and C_3) in the Sudakov exponent and in the $C_{ij}^{(n)}$ functions [7].

In Eq. (2), the impact parameter b is to be integrated from 0 to ∞. However, for $b \geq b_{\max}$, which corresponds to an energy scale less than $1/b_{\max}$, the QCD coupling $\alpha_s(\bar{\mu} \sim 1/b)$ becomes so large that a perturbative calculation is no longer reliable, and nonperturbative physics must set in. The nonperturbative physics in this region is described by an empirically fit function $\widetilde{W}_{ij}^{NP}$ [9,20], and $\widetilde{W}_{ij}$ is evaluated at a revised value of b, $b_* = b/\sqrt{1+(b/b_{\max})^2}$, where $b_{\max}$ is a phenomenological parameter used to separate long and short distance physics. With this change of variable, b_* never exceeds $b_{\max}$; $b_{\max}$ is a free parameter of the formalism [7] that can be constrained by other data (e.g. Drell-Yan).

The function Y in Eq. (2) contains contributions in the full NLO perturbative calculation that are less singular than Q_T^{-2} or $Q_T^{-2}\ln(Q^2/Q_T^2)$ as $Q_T \to 0$ (both the factorization and the renormalization scales are chosen to be C_4Q). It is the difference between the exact perturbative result to a given order and the result from $\widetilde{W}_{ij}$ expanded to the same fixed order (called the asymptotic piece). The function Y restores the regular contribution in the fixed order perturbative calculation that is not included in the resummed piece $\widetilde{W}_{ij}$. It does not contain a contribution from final-state fragmentation, which is included separately as described in Sec. III B.

The CSS formula Eq. (2) contains many higher-order logarithmic terms, such that when $Q_T \sim Q$, the resummed differential cross section can become negative in some regions of phase space. In this calculation, the fixed-order prediction for the differential cross section is used for $Q_T \gtrsim Q$ whenever it is larger than the prediction from Eq. (2). The detailed properties of this matching prescription can be found in Ref. [10].

A. Resummation for the $q\bar{q} \to \gamma\gamma$ subprocess

For the $q\bar{q} \to \gamma\gamma$ subprocess, the application of the CSS resummation formalism is similar to the Drell-Yan case $q\bar{q}^{(\prime)} \to V^* \to l_1\bar{l}_2$, where l_1 and l_2 are leptons produced through a gauge boson V^* [10]. Since both processes are initiated by $q\bar{q}^{(\prime)}$ color singlet states, the $A^{(1)}$, $A^{(2)}$ and $B^{(1)}$ functions in the Sudakov form factor are identical to those of the Drell-Yan case when each photon is in the central rapidity region with large transverse momentum and is well separated from the other photon. This universality can be understood as follows. The invariants $\hat{s}$, $\hat{t}$ and $\hat{u}$ are defined for the $q(p_1)\bar{q}(p_2) \to \gamma(p_3)\gamma(p_4)$ subprocess as

$$\hat{s} = (p_1+p_2)^2, \quad \hat{t} = (p_1-p_3)^2, \quad \hat{u} = (p_2-p_3)^2. \tag{6}$$

The transverse momentum of each photon can be written as $p_T^\gamma = \sqrt{\hat{t}\hat{u}/\hat{s}}$. When p_T^γ is large, $\hat{t}$ and $\hat{u}$ must also be large, and so the virtual-quark line connecting the two photons is far off the mass shell, and the leading logarithms due to soft gluon emission beyond the leading order can be generated only from diagrams in which soft gluons are connected to the incoming (anti-)quark. To obtain the $B^{(2)}$ function, it is necessary to calculate beyond NLO; so it is not included in this calculation. However, the Sudakov form factor becomes more accurate when more terms are included in A_{ij} and B_{ij}. Since the universal functions $A_{ij}^{(n)}$ depend only on the flavor of the incoming partons (quarks or gluons), $A_{qq}^{(2)}$ can be appropriated from Drell-Yan studies, and its contribution *is* included in this paper.

To describe the effects of multiple soft-gluon emission, Eq. (2) can be applied, where i and j represent quark and anti-quark flavors, respectively, and $\mathcal{F}_{ij} = \delta_{ij}(g_L^2+g_R^2)^2(1$

$+\cos^2\theta)/(1-\cos^2\theta)$. The couplings $g_{L,R}$ are defined through the $q\bar{q}\gamma$ vertex, written as $i\gamma_\mu[g_L(1-\gamma_5)+g_R(1+\gamma_5)]$, with $g_L=g_R=eQ_f/2$, and eQ_f is the electric charge of the incoming quark ($Q_u=2/3$, $Q_d=-1/3$). The explicit forms of the A and B functions are

$$A_{qq}^{(1)}(C_1)=C_F,$$

$$A_{qq}^{(2)}(C_1)=C_F\left[\left(\frac{67}{36}-\frac{\pi^2}{12}\right)N_C-\frac{5}{18}N_f-2\beta_1\ln\left(\frac{b_0}{C_1}\right)\right],$$

$$B_{qq}^{(1)}(C_1,C_2)=C_F\left[-\frac{3}{2}-2\ln\left(\frac{C_2b_0}{C_1}\right)\right], \tag{7}$$

where N_f is the number of light quark flavors, $N_C=3$, $C_F=4/3$, and $\beta_1=(11N_C-2N_f)/12$.

To obtain the value of the total cross section to NLO, it is necessary to include the Wilson coefficients $C_{ij}^{(0)}$ and $C_{ij}^{(1)}$. These can be derived from the full set of LO contributions and NLO corrections to $\gamma\gamma$ production [3]. After the leading order and the one-loop virtual corrections to $q\bar{q}\to\gamma\gamma$ and the tree level contribution from $q\bar{q}\to\gamma\gamma g$ are included, the coefficients are

$$C_{jk}^{(0)}\left(z,b,\mu,\frac{C_1}{C_2}\right)=\delta_{jk}\delta(1-z),$$

$$C_{jG}^{(0)}\left(z,b,\mu,\frac{C_1}{C_2}\right)=0,$$

$$C_{jk}^{(1)}\left(z,b,\mu,\frac{C_1}{C_2}\right)=\delta_{jk}C_F\left\{\frac{1}{2}(1-z)-\frac{1}{C_F}\ln\left(\frac{\mu b}{b_0}\right)P_{j\leftarrow k}^{(1)}(z)+\delta(1-z)\left[-\ln^2\left(\frac{C_1}{b_0C_2}\,e^{-3/4}\right)+\frac{\mathcal{V}}{4}+\frac{9}{16}\right]\right\}. \tag{8}$$

After factorization of the final-state collinear singularity, as described below, the real emission subprocess $qg\to\gamma\gamma q$ yields

$$C_{jG}^{(1)}\left(z,b,\mu,\frac{C_1}{C_2}\right)=\frac{1}{2}z(1-z)-\ln\left(\frac{\mu b}{b_0}\right)P_{j\leftarrow G}^{(1)}(z). \tag{9}$$

In the above expressions, the splitting kernels [19] are

$$P_{j\leftarrow k}^{(1)}(z)=C_F\left(\frac{1+z^2}{1-z}\right),$$

$$P_{j\leftarrow G}^{(1)}(z)=\frac{1}{2}[z^2+(1-z)^2]. \tag{10}$$

For photon pair production, the function $\mathcal{V}$ is

$$\mathcal{V}_{\gamma\gamma}=-4+\frac{\pi^2}{3}+\frac{\hat{u}\hat{t}}{\hat{u}^2+\hat{t}^2}[F^{virt}(v)-2],$$

$$F^{virt}(v)=\left(2+\frac{v}{1-v}\right)\ln^2(v)+\left(2+\frac{1-v}{v}\right)\ln^2(1-v)+\left(\frac{v}{1-v}+\frac{1-v}{v}\right)\left(\ln^2(v)+\ln^2(1-v)-3+\frac{2\pi^2}{3}\right)+2[\ln(v)+\ln(1-v)+1]+3\left(\frac{v}{1-v}\ln(1-v)+\frac{1-v}{v}\ln(v)\right), \tag{11}$$

where $v=-\hat{u}/\hat{s}$, and $\hat{u}=-\hat{s}(1+\cos\theta)/2$ in the $q\bar{q}$ center-of-mass frame. Because of Bose symmetry, $F^{virt}(v)=F^{virt}(1-v)$. A major difference from the Drell-Yan case ($\mathcal{V}_{DY}=-8+\pi^2$) is that $\mathcal{V}_{\gamma\gamma}$ depends on the kinematic correlation between the initial and final states through its dependence on $\hat{u}$ and $\hat{t}$.

The nonperturbative function used in this study is the empirical fit [20]

$$\widetilde{W}_{qq}^{NP}(b,Q,Q_0,x_1,x_2)=\exp\left[-g_1b^2-g_2b^2\ln\left(\frac{Q}{2Q_0}\right)-g_1g_3b\ln(100x_1x_2)\right], \tag{12}$$

where $g_1=0.11^{+0.04}_{-0.03}$ GeV^2, $g_2=0.58^{+0.1}_{-0.2}$ GeV^2, $g_3=-1.5^{+0.1}_{-0.1}$ GeV^{-1}, and $Q_0=1.6$ GeV. (The value $b_{max}=0.5$ GeV^{-1} was used in determining the above g_i's and for the numerical results presented in this paper.) These values were fit for the CTEQ2M parton distribution function, with the conventional choice of the renormalization constants, i.e. $C_1=C_3=b_0$ and $C_2=1$. In principle, these coefficients should be refit for the CTEQ4M distributions [24] used in this study. The parameters of Eq. (12) were determined from Drell-Yan data. It is assumed that the same values should be applicable for the $\gamma\gamma$ final state.

B. Contributions from qg subprocesses

As described in Sec. II, the complete NLO calculation of diphoton production in hadron collisions includes photons from long-distance fragmentation processes like Fig. 1(b) and short-distance processes like Figs. 1(f) and 1(g). The latter processes yield a regular 3-body final state contribution, while the former describes a photon recoiling against a collinear quark and photon.

The singular part of the squared amplitude of the $q(p_1)g(p_2)\to\gamma(p_3)\gamma(p_4)q(p_5)$ subprocess can be factored into a product of the squared amplitude of $q(p_1)g(p_2)\to\gamma(p_3)q(p_{4+5})$ and the splitting kernel for $q(p_{4+5})\to\gamma(p_4)q(p_5)$. In the limit that the emitted photon $\gamma(p_4)$ is collinear with the final state quark $q(p_5)$

$$\lim_{p_4\| p_5}|\mathcal{M}[q(p_1)g(p_2)\to\gamma(p_3)\gamma(p_4)q(p_5)]|^2=\frac{e^2}{p_4\cdot p_5}P_{\gamma\leftarrow q}^{(1)}(z)|\mathcal{M}[q(p_1)g(p_2)\to\gamma(p_3)q(p_{4+5})]|^2. \tag{13}$$

A similar result holds when p_3 and p_5 become collinear and/or the quark is replaced with an anti-quark. Conventionally, the splitting variable z is the light-cone momentum fraction of the emitted photon with respect to the fragmenting quark, $z=p_4^+/(p_4^++p_5^+)$, where $p_i^+=(p_i^{(0)}+p_i^{(3)})/\sqrt{2}$. ($p_i^{(0)}$ is the energy and $p_i^{(3)}$ is the longitudinal momentum component along the moving direction of the fragmenting quark in the qg center-of-mass frame.) Alternatively, since the final state under consideration contains only a fragmenting quark and a spectator, a Lorentz invariant splitting variable can be defined as [21]

$$\tilde{z}=1-\frac{p_i\cdot p_k}{p_j\cdot p_k+p_i\cdot p_k+p_i\cdot p_j}. \tag{14}$$

In this notation, $i=5$ is the fragmentation quark, j is the fragmentation photon, and k is the prompt spectator photon. When the pair ij becomes collinear, $\tilde{z}$ becomes the same as the light-cone momentum fraction z carried by the photon. Aside from the color factor, $P^{(1)}_{\gamma\leftarrow q}(z)$ in Eq. (13) is the usual Dokshitzer-Gribov-Lipatov-Altarelli-Parisi (DGLAP) splitting kernel for $q\rightarrow gq$:

$$P^{(1)}_{\gamma\leftarrow q}(z)=\left(\frac{1+(1-z)^2}{z}\right). \tag{15}$$

The regular contribution $qg\rightarrow\gamma\gamma q$ [Fig. 1(f)] is defined by removing the final-state, collinear singularity from the full amplitude of the partonic subprocess. The matrix element squared for Fig. 1(f) can be written [21]

$$|\mathcal{M}(qg\rightarrow\gamma\gamma q)|^2_{reg}=|\mathcal{M}(qg\rightarrow\gamma\gamma q)|^2_{full}-\frac{e^2}{p_4\cdot p_5}P^{(1)}_{\gamma\leftarrow q}(\tilde{z})|\mathcal{M}[q(p_1)g(p_2)\rightarrow\gamma(p_3)q(p_{4+5})]|^2. \tag{16}$$

After the final-state collinear singularity is subtracted, the remainder expresses the regular 3-body final state contribution $\gamma\gamma q$. This remainder, as shown in Fig. 1(g), contains terms that diverge when $Q_T\rightarrow 0$ which should be regulated by renormalizing the parton distribution at NLO. The contribution from this divergent part is included in the resummed $q\bar{q}$ cross section in $C^{(1)}_{jG}$, as shown in Eq. (9). The part that is finite as $Q_T\rightarrow 0$ is included in the function Y. When $Q_T\gtrsim Q$, Eq. (16) describes the NLO contribution from the $qg\rightarrow\gamma\gamma q$ subprocess to the Q_T distribution of the photon pair. The subtracted final-state collinear singularity from the NLO $qg\rightarrow\gamma\gamma q$ subprocess is absorbed into the fragmentation process 1(b).

C. Fragmentation contributions

Final-state photon fragmentation functions $D_{\gamma/i}(z,\mu_F^2)$ are introduced in an analogous manner to initial-state parton distribution functions $f_{i/h_1}(x,\mu_I^2)$. Here, $z(x)$ is the light-cone momentum fraction of the fragmenting quark (incident hadron) carried by the photon (initial-state parton), and $\mu_F(\mu_I)$ is the final state (initial state) fragmentation (factorization) scale. The parton-level cross section for the fragmentation contribution 1(b) is evaluated from the general expression for a hard scattering to a parton m, which then fragments to a photon:

$$d\hat{\sigma}=\frac{1}{2\hat{s}}|\mathcal{M}(p_1p_2\rightarrow p_3\ldots p_m)|^2d^{(m-2)}[PS]dzD_{\gamma/m}(z,\mu_F^2). \tag{17}$$

Here, $\mathcal{M}$ is the matrix element for the hard scattering subprocess, $d^{(m-2)}[PS]$ is the $m-2$-body phase space, and an integral is performed over the photon momentum fraction z weighted by the fragmentation function $D_{\gamma/m}(z,\mu_F^2)$. Since fragmentation is computed here to LO only, the infrared divergences discussed by Berger, Guo and Qiu are not an issue [22].

The fragmentation function $D_{\gamma\leftarrow q}$ obeys an evolution equation, and the leading-logarithm, asymptotic solution $D^{LL}_{\gamma/q}$ is [3]

$$D^{LL}_{\gamma/q}(z,\mu_F^2)=\frac{\alpha_{em}}{2\pi}\ln\left(\frac{\mu_F^2}{\Lambda^2_{QCD}}\right)D^{(1)}_{\gamma\leftarrow q}(z),$$

$$zD^{(1)}_{\gamma\leftarrow q}(z)=\frac{Q_q^2(2.21-1.28z+1.29z^2)z^{0.049}}{1-1.63\,\ln(1-z)}+0.0020(1-z)^{2.0}z^{-1.54}, \tag{18}$$

where Λ_{QCD} is the QCD scale for four light quark flavors. As shown in Fig. 2, the collinear approximation made in defining $D_{\gamma\leftarrow q}$ leads to kinematic distributions with an unrealistic sensitivity to kinematic cuts, such as cuts to define an isolated photon.

The Monte Carlo showering method goes beyond the collinear approximation used in solving the evolution equation for the fragmentation function $D_{\gamma\leftarrow q}$. In Monte Carlo calculations, the probability for photon emission is determined from the splitting function $P_{\gamma\leftarrow q}(z)$, which is a collinear approximation. However, the kinematics is treated by assigning a virtuality to the fragmenting quark whose value lies between the hard scale of the process and a phenomenological cutoff ~ 1 GeV. This cutoff replaces the parameter Λ_{QCD} in Eq. (18). Most importantly, gluon emission can be incorporated into the description of final state fragmentation. Because there is no collinear approximation in the kinematics, kinematic distributions do not exhibit the unrealistic behavior of the parton-level calculation. The ''correctness'' of either approach can be judged only after a careful comparison of their respective predictions.

The collinear approximation becomes an issue because of the experimental definition of isolated photons. Experimentally, an isolation cut is necessary to separate prompt photons from various hadronic backgrounds, including π^0 and η meson decays. The separation between a particle j and the photon is expressed as $R_j=\sqrt{(\eta-\eta_j)^2+(\phi-\phi_j)^2}$, where the coordinates $\eta(\eta_j)$ and $\phi(\phi_j)$ are the pseudorapidity and azimuthal angle of the photon (particle j). At hadron colliders, the standard isolation criterion is that the sum of excess transverse energy E_T contained inside a cone of size R_0 centered on the photon candidate is below a cutoff E_T^{iso}, $\Sigma_{R_j<R_0}E_T^j<E_T^{iso}$. The sum is over each particle j. Since the

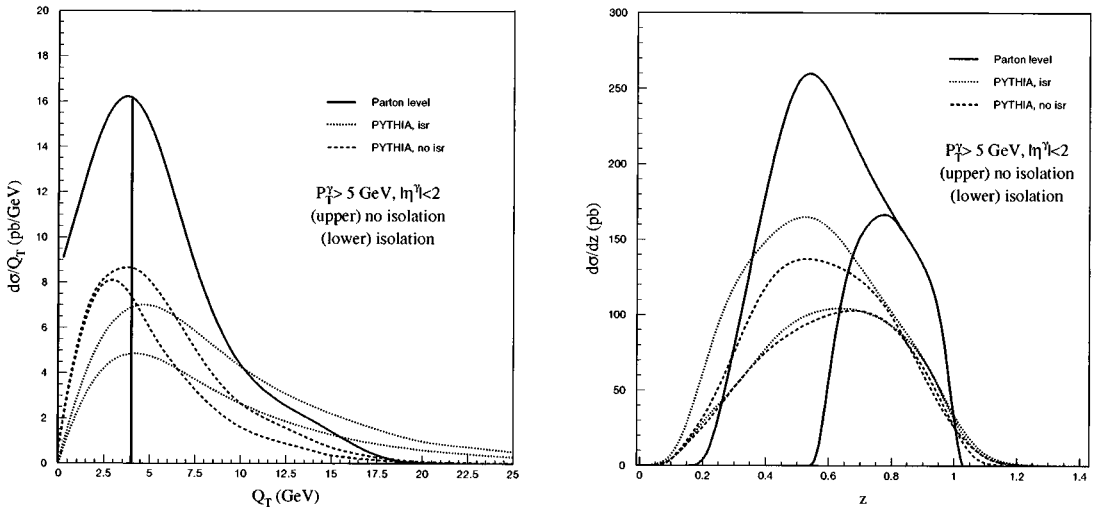

FIG. 2. Comparison of the parton-level and Monte Carlo fragmentation contributions at the Tevatron. The upper and lower curves of the same type show the contribution before and after an isolation cut. The left figure shows the transverse momentum of the photon pair Q_T. The right figure shows the light-cone momentum fraction carried by the fragmentation photon.

resummed CSS piece of the final state cross section describes the radiation of multiple soft gluons approximately collinear with the incident partons, it produces only isolated photons. For NLO $\gamma\gamma j$ final states 1(e), 1(f), and 1(g), where there is only one extra parton $j=q$ or g, isolation enforces a separation $R_j \geqslant R_0$, provided that $p_{T_j} > E_T^{iso}$. Above $Q_T = E_T^{iso}$, the perturbative corrections contained in the function Y are affected by isolation. On the other hand, because of the collinear approximation, the parton-level fragmentation calculation based on Eq. (18) does not depend on the isolation cone R_0; the hadronic remnant of the fragmentation 1(b) *always* satisfies $R < R_0$. Hence, for this case, $\vec{Q}_T = (1-z)\vec{p}_{T_1}$, and the isolation cut reduces to a step function requirement $\theta(E_T^{iso} - Q_T)$.

The parton-level calculation of the fragmentation contribution at the Tevatron based on the fragmentation function $D_{\gamma \leftarrow q}(z, \mu_F^2)$ has been compared with a Monte Carlo estimate based on PYTHIA [23]. For the parton-level calculation, the scale $\mu_F = M_{\gamma\gamma}$ is used. For the PYTHIA calculation, the scale is $\mu_F = \sqrt{\hat{s}}$, and hadronization is not performed, so that no photons arise from π^0 or η meson decays, for example. For this comparison, the invariant mass $\sqrt{\hat{s}}$ of the hard-scattering subprocess is limited to $20 < \sqrt{\hat{s}} < 50$ GeV in both approaches, and the photons are required to satisfy $p_T^\gamma > 5$ GeV and $|\eta^\gamma| < 2$. These kinematic cuts are chosen to increase the statistics of the PYTHIA calculation, while reflecting the kinematic region of interest for a comparison with data. PYTHIA can simulate the QED and QCD showering of the final-state quark as well as the QCD showering of the initial-state quark and gluon. To isolate the effect of initial-state gluon radiation, PYTHIA calculations were performed with and without the QCD initial-state radiation (i.e. by preventing space-like showering). In neither case is initial-state QED radiation simulated. It is possible for the partons produced in initial-state showering to develop time-like showering. Any photons produced from this mechanism are discarded, since they are formally of higher order than the contributions considered here. Such contributions, however, might be necessary to understand photon pairs with small invariant mass and small Q_T.

Figure 2 is a comparison of kinematic quantities from the parton-level and Monte Carlo calculations. The left side of Fig. 2 shows the Q_T distribution for the parton level (solid), PYTHIA with initial-state radiation of gluons (short-dashed line), and PYTHIA without initial-state radiation (long-dashed line) calculations. Each curve is plotted twice, with and without an isolation cut $E_T^{iso} = 4$ GeV and $R_0 = 0.7$. Before the isolation cut, the total parton-level fragmentation cross section is approximately 50% higher than the Monte Carlo cross section. After isolation, the total cross sections are in good agreement, even though the parton-level calculation is discontinuous at $Q_T = E_T^{iso}$. The effect of initial-state gluon radiation in the PYTHIA calculation is to increase Q_T without compromising the isolation of the photons.

The right side of Fig. 2 shows the distribution of the light-cone momentum fraction z of the quark carried by the fragmentation photon (for this figure, z is defined in the laboratory frame). After isolation, the parton-level contribution is limited to $z > 0.55$ by kinematics, whereas the Monte Carlo contribution is more uniformly distributed between 0 and 1. For the PYTHIA result, z is calculated with respect to the final state quark *before* showering. In the showering process, some energy-momentum can be exchanged between the final state prompt photon and the fragmenting quark, since the quark is assigned a virtuality. As a result, the effective z value can extend beyond the naive limit $z = 1$.

The conclusions of this comparison are as follows: (1) after isolation, the total cross sections from the parton-level and Monte Carlo fragmentation calculations are in good agreement, and (2) the Monte Carlo kinematic distributions (e.g. Q_T and z) are not very sensitive to the isolation cut. For these reasons, the Monte Carlo estimate with initial-state radiation is used to account for the contribution of Fig. 1(b) in the final results. Furthermore, with initial-state radiation, the PYTHIA calculation includes the leading effects of a full re-

summation calculation of the $qg \to \gamma q$ process. It is approximately equivalent to performing a resummation calculation in the CSS formalism with quantities $A^{(1)}$ and $B^{(1)}$ calculated for a qg initial state and the LO Wilson function.

One final comparison was made with the Monte Carlo calculation by treating the subtracted term in Eq. (16), with $P^{(1)}$ replaced by $D^{(1)}$ defined in Eq. (18), as a 3-body matrix element. The collinear divergence was regulated by requiring a separation R_0 between the photon and quark remnant for all Q_T. This calculation agrees with PYTHIA in the shape and normalization of various distributions, except when $Q_T < E_T^{iso}$, where there is a substantial difference.

D. Resummation for the $gg \to \gamma\gamma$ subprocess

A resummation calculation for the $gg \to \gamma\gamma$ subprocess is included in the theoretical prediction. The LO contribution comes from one-loop box diagrams of order $\alpha_{em}^2 \alpha_s^2$ in perturbative QCD. At present, a full NLO calculation, of $\mathcal{O}(\alpha_{em}^2 \alpha_s^3)$, for this process is not available. Nevertheless, the resummation technique can be applied to resum part of the higher order contributions and improve the theoretical prediction. The exact NLO $gg \to \gamma\gamma g$ calculation must include gluon emission from the internal quark lines of the box diagram, thus generating pentagon diagrams. However, such diagrams do not generate large logarithms when the final state photons have large transverse momentum, are in the central rapidity region, and are well separated from each other. All the large logarithms originate from the diagrams with soft gluons coupling to the initial-state gluons. Similarly, the exact NLO $qg \to \gamma\gamma q$ calculation, of $\mathcal{O}(\alpha_{em}^2 \alpha_s^3)$, must include contributions involving a box diagram with one incoming gluon off shell. Large logarithms only arise from soft gluon emission off the initial-state quark or gluon. The leading logarithms due to initial-state radiation are universal, and the $A^{(1)}$ function calculated for the resummed $gg \to H$ process [11,12] or the $gg \to Q\overline{Q}$ process [13] can be applied directly to the resummed $gg \to \gamma\gamma$ calculation, since these subprocesses have the same QCD color structure.

When the transverse momentum of the photon pair is much smaller than its invariant mass, i.e. $Q_T \ll Q$, and each photon has large transverse momentum, then the box diagram of the hard scattering subprocess $gg \to \gamma\gamma$ can be approximated as a point-like interaction (multiplied by a form factor which depends on $\hat{s}$, $\hat{t}$ and $\hat{u}$). This approximation ignores pentagon diagrams in the $gg \to \gamma\gamma g$ subprocess and the virtuality of intermediate quarks in the $qg \to \gamma\gamma q$ subprocess. It does not have the complete structure of the hard process, but it does contain the most important logarithmic terms from initial state gluon radiation. Under such an approximation, the subleading logarithmic terms associated with $B^{(1)}$, $A^{(2)}$, and $C^{(1)}$ of Eqs. (4) and (5) can be included in the resummation calculation. These functions were calculated for the $gg \to H$ process [11,12]. Without a complete $\mathcal{O}(\alpha_{em}^2 \alpha_s^3)$ calculation, the exact Wilson coefficient function $C^{(1)}$ is not known. Since part of the exact $C^{(1)}$ function must include the piece for the $gg \to H$ process, it is included to estimate the possible NLO enhancement to the production rate of the gg subprocess. After these ingredients are incorporated into Eq. (2), the resummed kinematics of the photon pair from the $gg \to \gamma\gamma$ subprocess can be obtained. The distribution of the individual photons can be calculated approximately from the LO angular dependence of the box diagram.

The above approximation certainly fails when Q_T is of the order of Q. In the absence of a complete $\mathcal{O}(\alpha_{em}^2 \alpha_s^3)$ calculation of the $gg \to \gamma\gamma g$ and $qg \to \gamma\gamma q$ subprocesses, it is not possible to estimate the uncertainties introduced by the approximation. In the limit of $Q_T \ll Q$, the approximation should be reliable, since the soft gluon approximation is applicable. In the same spirit, the approximate function Y for photon pair production is taken from the results of the perturbative piece for the $gg \to Hg$ and $gq \to Hq$ processes [11,12].

In summary, the resummed distributions of the photon pair from the gg subprocess in the region of $Q_T \ll Q$ can be described by Eq. (2), with $i=j=g$, and $\mathcal{F}_{gg} = N_C |\mathcal{M}_{gg\to\gamma\gamma}(s,t,u)|^2/2^{12}$. Here, $|\mathcal{M}_{gg\to\gamma\gamma}(s,t,u)|^2$ is the absolute square of the invariant amplitude of the $gg \to \gamma\gamma$ subprocess [2] summed over spins, colors, and the fermion flavors in the box loop, but without the initial-state color $(1/8^2)$, spin $(1/2^2)$ average, and the final-state identical particle $(1/2)$ factors. The A and B functions used in the calculation for the gg initial state are

$$A_{gg}^{(1)}(C_1) = C_A = 3,$$

$$A_{gg}^{(2)}(C_1) = \frac{C_A}{C_F} A_{qq}^{(2)}(C_1),$$

$$B_{gg}^{(1)}(C_1, C_2) = 2\left[3 \ln\left(\frac{C_1}{C_2 b_0} \right) - \beta_1 \right]. \tag{19}$$

The LO and NLO Wilson coefficients, extracted from the $gg \to H$ subprocess, are

$$C_{gg}^{(0)}\left(z, b; \frac{C_1}{C_2}; \mu \right) = \delta(1-z),$$

$$C_{qg}^{(0)}\left(z, b; \frac{C_1}{C_2}; \mu \right) = 0,$$

$$C_{gg}^{(1)}\left(z, b; \frac{C_1}{C_2}; \mu \right) = -\ln\left(\frac{\mu b}{b_0} \right) P_{g\leftarrow g}(z) + \delta(1-z) \times \left\{ \frac{11}{4} + \frac{3\pi^2}{4} - 3\ln^2\left(\frac{C_1}{C_2 b_0} \right) + 3\ln\left(\frac{C_1}{C_2 b_0} \right) + (2\beta_1 - 3)\ln\left(\frac{\mu b}{b_0} \right) \right\},$$

$$C_{qg}^{(1)}\left(z, b; \frac{C_1}{C_2}; \mu \right) = -\ln\left(\frac{\mu b}{b_0} \right) P_{g\leftarrow q}(z) + \frac{2}{3} z. \tag{20}$$

Since the NLO pentagon and off-shell box diagram calculations are not included, the Wilson coefficients $C_{ij}^{(1)}$ are expected to predict accurately the total cross section only when $Q_T \ll Q$, the transverse momenta of the individual photons are large, and their rapidities are small. Under the *approximation* made above, the resummed gg result increases

the integrated rate by about a factor of 2, for kinematic cuts typical of the Tevatron, as compared to the lowest order (one-loop calculation) perturbative result. This comparison suggests that the full NLO contribution of the gg initiated subprocess is large. Because it is necessary to impose the condition $Q_T < Q$ to make the above approximations valid, the gg resummed result presented in this work probably underestimates the rate when Q_T is large or the separation of the azimuthal angle ($\Delta\phi$) between the two photons is small. This deficiency can be improved only by a complete $\mathcal{O}(\alpha_{em}^2\alpha_s^3)$ calculation.

At the Tevatron, the gg contribution is important when the invariant mass ($M_{\gamma\gamma}=Q$) of the two photon pair is small. Because of the approximation made in the gg calculation beyond LO, the prediction will be more reliable for the data with larger Q. A more detailed discussion is presented in the next section.

The full calculation of the gg contribution in the CSS formalism depends also upon the choice of nonperturbative functions. However, the best fits to the parametrizations are performed for $q\bar{q}$ processes [9,20]. Two assumptions were studied: (i) the nonperturbative functions are truly universal for $q\bar{q}$ and gg processes, and (ii) the nonperturbative functions obey the same renormalization group properties as the A functions for each type of process (which are universal for all $q\bar{q}$ or gg subprocesses), and so the coefficient of the $\ln(Q/2Q_0)$ term in the nonperturbative function (12) is scaled by C_A/C_F relative to that of the $q\bar{q}$ process. Specifically, the different assumptions are

$$\text{(i)}\quad \tilde{W}_{gg}^{NP}(b,Q,Q_0,x_1,x_2)=\tilde{W}_{q\bar{q}}^{NP}(b,Q,Q_0,x_1,x_2),$$

$$\text{(ii)}\quad \tilde{W}_{gg}^{NP}(b,Q,Q_0,x_1,x_2)=\tilde{W}_{q\bar{q}}^{NP}(b,Q,Q_0,x_1,x_2),\quad \left(g_2\rightarrow\frac{C_A}{C_F}g_2\right). \tag{21}$$

The numerical values of g_1, g_2, and g_3 are listed following Eq. (12). These two assumptions do not exhaust all possibilities but ought to be representative of reasonable choices. Choice (ii) is used for the results presented in this paper. The effect of different choices is discussed in Sec. IV.

IV. NUMERICAL RESULTS

A. Tevatron collider energies

Two experimental collaborations at the Tevatron $p\bar{p}$ collider have collected diphoton data at $\sqrt{S}=1.8$ TeV: CDF [15], with 84 pb^{-1}, and DØ [16], with 81 pb^{-1}. The kinematic cuts applied to the resummed prediction for comparison with the CDF data are $p_T^{\gamma}>12$ GeV and $|\eta^{\gamma}|<0.9$. For DØ, the kinematic cuts are $p_T^{\gamma_1}>14$ GeV and $p_T^{\gamma_2}>13$ GeV, and $|\eta^{\gamma}|<1$. For CDF, an isolation cut for each photon of $R_0=0.7$ and $E_T^{iso}=4$ GeV is applied; for DØ, the cut is $R_0=0.4$ and $E_T^{iso}=2$ GeV.

Other ingredients of the calculation are (i) the CTEQ4M parton distribution functions, (ii) the NLO expression for α_s, (iii) the NLO expression for α_{em}, and (iv) the nonperturbative coefficients of Ladinsky and Yuan [20].

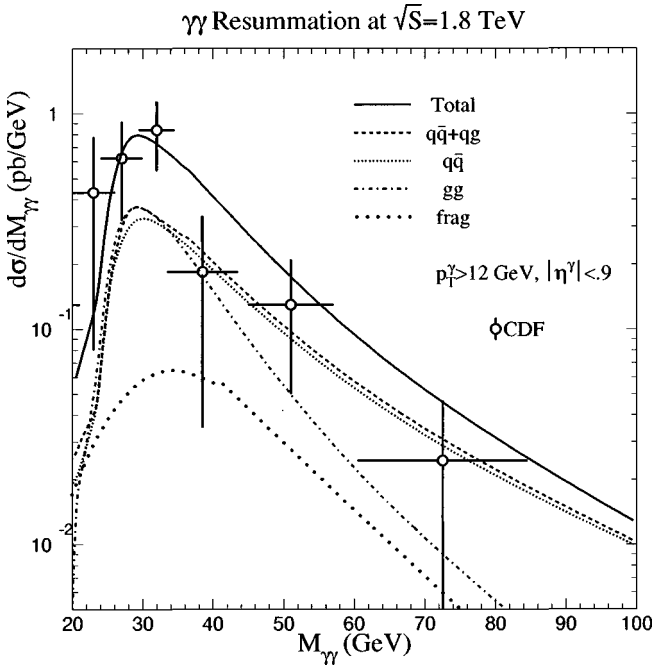

FIG. 3. The predicted distribution for the invariant mass of the photon pair $M_{\gamma\gamma}$ from the resummed calculation compared to the CDF data, with the CDF cuts imposed in the calculation.

The predictions for the CDF cuts and a comparison to the data are shown in Figs. 3–5. Figure 3 shows the distribution of the photon pair invariant mass, $d\sigma/dM_{\gamma\gamma}$ vs $M_{\gamma\gamma}$. The dot-dashed curve represents the resummation of the gg subprocess, which is the largest contribution for $M_{\gamma\gamma}\lesssim 30$ GeV. The long-dashed curve represents the full $q\bar{q}$ resummation, while the short-dashed curve is a similar calculation with the gluon parton distribution function artificially set to zero. Schematically, there are contributions to the resummed calculation that behave like $q\rightarrow gq_1\otimes q_1\bar{q}\rightarrow\gamma\gamma$ and $g\rightarrow\bar{q}q_1\otimes q_1\bar{q}\rightarrow\gamma\gamma$. These contributions are contained in the terms proportional to $P_{j\leftarrow k}^{(1)}(z)$ in Eq. (8) and $P_{j\leftarrow G}^{(1)}(z)$ in Eq. (9), respectively. The full $q\bar{q}$ resummation contains both the $q\bar{q}$ and qg contributions. The short-dashed curve is calculated by setting $C_{jG}^{(1)}=0$ and retaining only the $q\bar{q}$ contribution in the function Y. Since the short-dashed curve almost saturates the full $q\bar{q}+qg$ contribution, except at large Q_T or small $\Delta\phi$, the qg initiated subprocess is not important at the Tevatron in most of phase space for the cuts used. The fragmentation contribution is denoted by the dotted line. The sum of all contributions including fragmentation is denoted by the solid line. After isolation, the fragmentation contribution is much smaller than ''direct'' ones, but contributes $\simeq 10\%$ near the peak. The uncertainty in the contribution of the fragmentation process can be estimated by comparing the Monte Carlo result with a parton-level calculation, as shown in Fig. 2.

Figure 4 shows the distribution of the transverse momentum of the photon pair, $d\sigma/dQ_T$ vs Q_T. Over the interval $5\lesssim Q_T\lesssim 25$ GeV, the contribution from the gg subprocess is comparable to the $q\bar{q}+qg$ subprocess. The change in slope near $Q_T=20$ GeV arises from the gg subprocess (dot-dashed line) for which $Q_T\lesssim M_{\gamma\gamma}$ is required in our approximate cal-

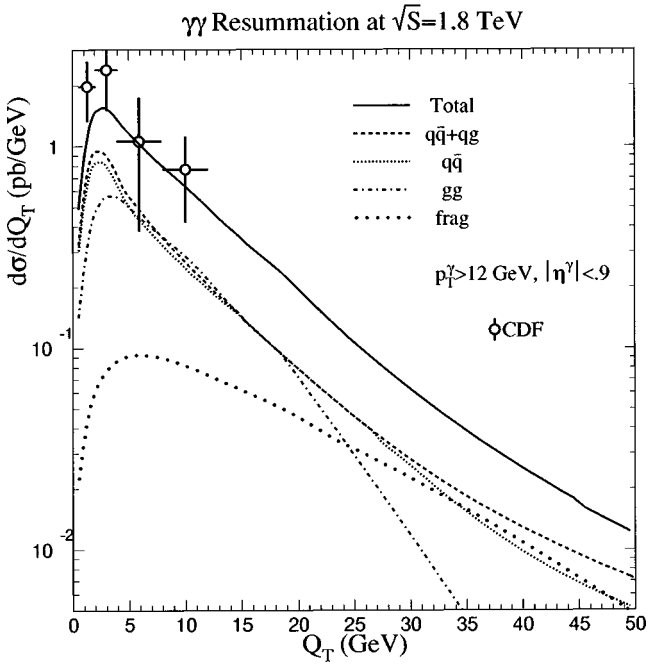

FIG. 4. The predicted distribution for the transverse momentum of the photon pair Q_T from the resummed calculation compared to the CDF data, with the CDF cuts imposed in the calculation.

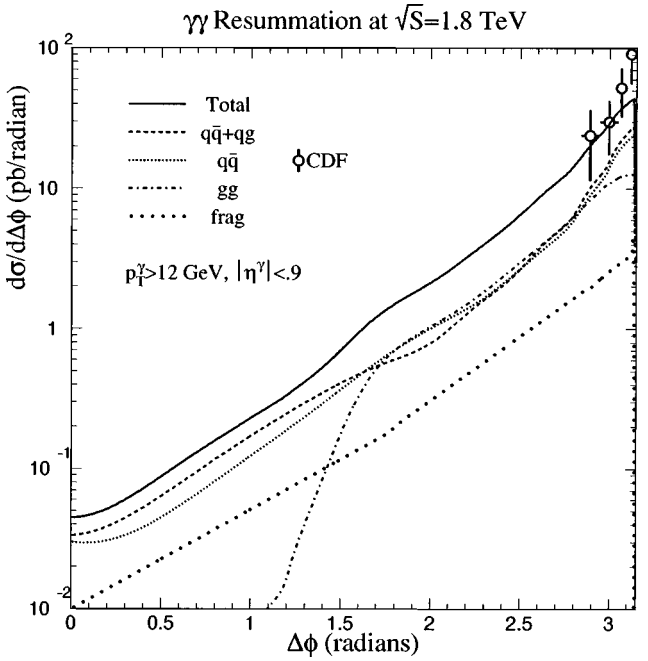

FIG. 5. The predicted distribution for the difference between the azimuthal angles of the photons $\Delta\phi_{\gamma\gamma}$ from the resummed calculation compared to the CDF data, with the CDF cuts imposed in the calculation.

culation. The peak near $Q_T \simeq 1.5$ GeV is provided mostly by the $q\bar{q}+qg$ (long-dashed line) subprocess. In general, the height and breadth of the peak in the Q_T distribution depend on the details of the nonperturbative function in Eq. (2). The effect of different nonperturbative contributions may be estimated if the parameter g_2 is varied by $\pm 2\sigma$. For $Q_T > 10$ GeV, the distribution is not sensitive to this variation. The height and the width (half-maximum) of the peak change by approximately 20% and 35%, respectively, but the integrated rate from 0 to 10 GeV is almost constant. The peak of the distribution (which is below 5 GeV) shifts approximately $+0.5$ GeV or -0.6 GeV for a $+2\sigma$ or -2σ variation. The mean Q_T for $Q_T < 10$ GeV shifts at most by 0.4 GeV. For gg resummation, it is not clear which parametrization of the nonperturbative physics should be used. However, the final effect of the two different parametrizations outlined in Eq. (21) is minimal, shifting the mean Q_T for $Q_T < 40$ GeV by about 0.4 GeV. The parametrization (ii) is used in the final results, so that the coefficient g_2 is scaled by C_A/C_F relative to the $q\bar{q}$ nonperturbative function.

Figure 5 shows $d\sigma/d\Delta\phi$ vs $\Delta\phi$, where $\Delta\phi$ is the azimuthal opening angle between the two photons. The change in slope near $\Delta\phi = \pi/2$ is another manifestation of the approximations made in the treatment of the gg contribution (dot-dashed line). The height of the distribution near $\Delta\phi \simeq \pi$ is also sensitive to the details of the nonperturbative function.

In the absence of resummation or NLO effects, the gg box contribution supplies $\vec{Q}_T = 0$ and $\Delta\phi = \pi$. In this calculation, as explained earlier, the NLO contribution for the gg subprocess is handled in an approximate fashion. For the cuts listed above, the total cross section from the complete gg resummed calculation, including the function Y, is 6.28 pb. If the resummed CSS piece is used alone, the contribution is reduced to 4.73 pb. This answer can be compared to the contribution at LO. For the same structure functions, the LO gg cross section for the CDF cuts is 3.18 pb for the scale choice $Q = M_{\gamma\gamma}$. Therefore, the effect of including part of the NLO contribution to the $\gamma\gamma$ process is to approximately double the LO gg box contribution to the cross section. This increase indicates that the exact NLO correction can be large for the gg subprocess and motivates a full calculation.

The predictions for the DØ cuts and a comparison to data are shown in Figs. 6–8. Because of the steep distribution in the transverse momentum of the individual photons, the higher p_T^γ threshold in the DØ case significantly reduces the total cross section. Otherwise, the behavior is similar to the resummed calculation shown for the CDF cuts. The DØ data plotted in the figures are not corrected for experimental resolution. To compare with the uncorrected DØ data with the kinematic cuts $p_T^{\gamma_1} > 14$ GeV, $p_T^{\gamma_2} > 13$ GeV and $\eta^\gamma < 1.0$, an ''equivalent'' set of cuts is used in the theoretical calculation: $p_T^{\gamma_1} > 14.9$ GeV, $p_T^{\gamma_2} > 13.85$ GeV, and $\eta^\gamma < 1.0$ [25]. The effect of this ''equivalent'' set is to reduce the theoretical rate in the small $M_{\gamma\gamma}$ region.

While the agreement in both shapes and absolute rates is generally good, there are some discrepancies between the resummed prediction and the data as presented in these plots. At small Q_T (Fig. 4) and large $\Delta\phi$ (Fig. 5), where the CDF cross section is large, the theoretical results are beneath the data. Since this is the kinematic region in which the nonperturbative physics is important, better agreement can be obtained if the nonperturbative function is altered. In Fig. 6, the calculated $M_{\gamma\gamma}$ distribution is larger than the DØ data at large $M_{\gamma\gamma}$, while the calculation appears to agree with the CDF data in Fig. 3. The small discrepancy in Fig. 6 at large values of $M_{\gamma\gamma}$ is not understood. (The systematic errors of the data, which are about 25% [25], are not included in this

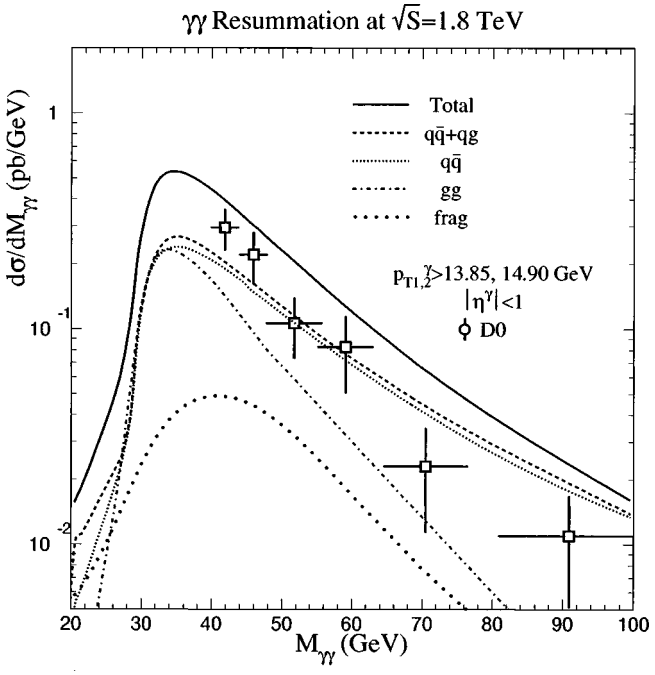

FIG. 6. The predicted distribution for the invariant mass of the photon pair $M_{\gamma\gamma}$ from the resummed calculation compared to the DØ data, with the DØ cuts imposed in the calculation.

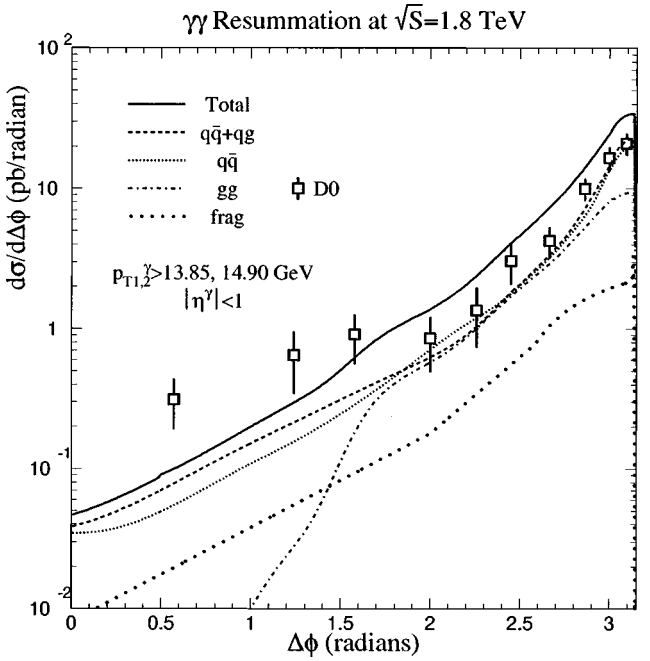

FIG. 8. The predicted distribution for the difference between the azimuthal angles of the photons $\Delta\phi_{\gamma\gamma}$ from the resummed calculation compared to the DØ data, with the DØ cuts imposed in the calculation.

plot.) On the other hand, Figs. 7 and 8 show that the resummed calculation is *beneath* the data at large Q_T or small $\Delta\phi$. The discrepancies in Figs. 7 and 8 may result from the approximations made in the gg process (notice the kinks in the dot-dashed curves). A complete NLO calculation for the gg subprocess is needed, and may improve the comparison with data for small $\Delta\phi$.

Because of the uncertainty in the prediction for the gg contribution of the resummed calculation, the distributions in $M_{\gamma\gamma}, Q_T$ and $\Delta\phi$ are shown in Figs. 9–11 for the CDF cuts and the additional requirement that $Q_T < M_{\gamma\gamma}$. This additional requirement should significantly reduce the theoretical uncertainty for large Q_T and small $\Delta\phi$. As remarked in Sec. II, in this work the contribution from double photon fragmentation initiated by the subprocess $gg \to q\bar{q}(g)$ is not included.

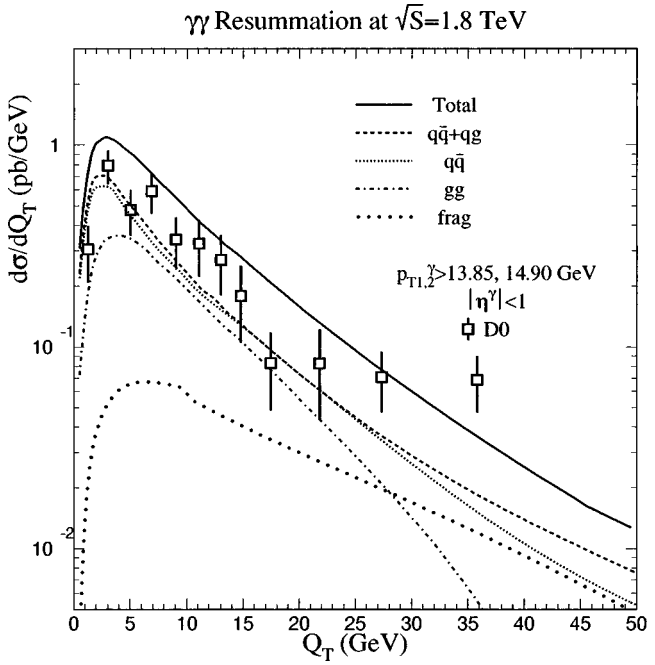

FIG. 7. The predicted distribution for the transverse momentum of the photon pair Q_T from the resummed calculation compared to the DØ data, with the DØ cuts imposed in the calculation.

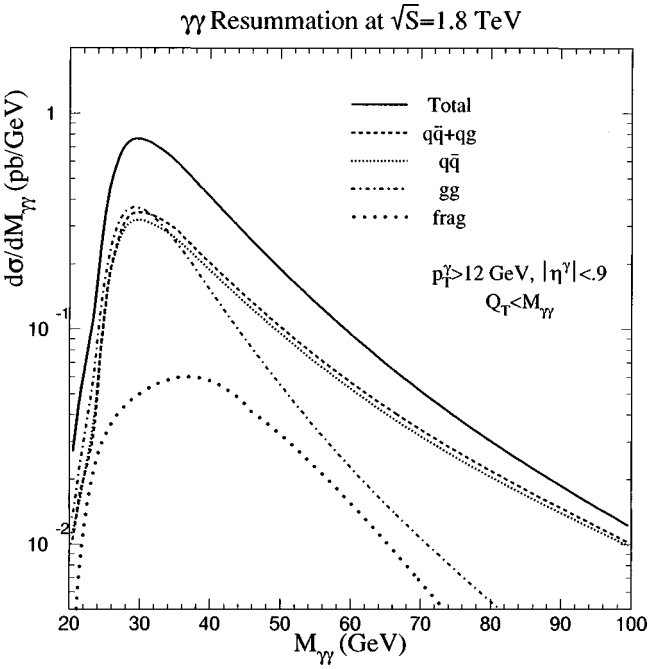

FIG. 9. The predicted distribution for the invariant mass of the photon pair $M_{\gamma\gamma}$ from the resummed calculation. The additional cut $Q_T < M_{\gamma\gamma}$ has been applied to reduce the theoretical uncertainty.

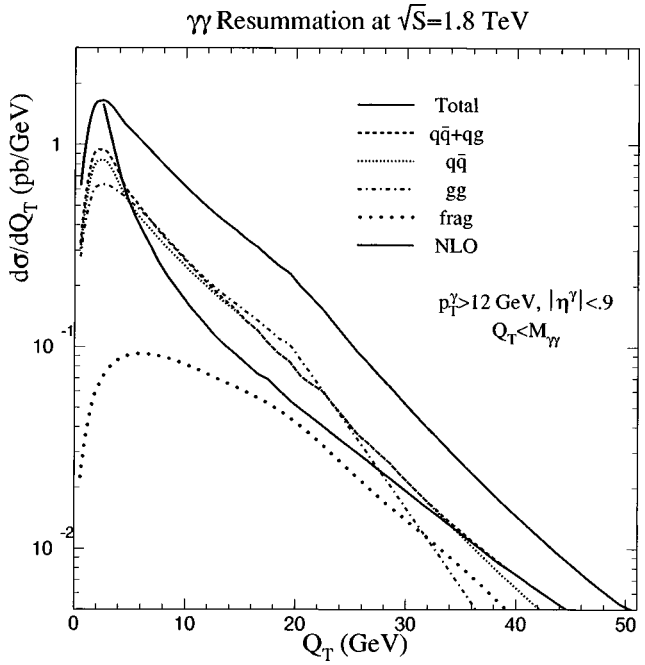

FIG. 10. The predicted distribution for the transverse momentum of the photon pair Q_T from the resummed calculation. The additional cut $Q_T < M_{\gamma\gamma}$ has been applied to reduce the theoretical uncertainty. The lower solid curve shows the prediction of the pure NLO (fixed-order) calculation for the $q\bar{q}$ and qg subprocesses, but without fragmentation contributions.

In Fig. 10, the lower of the two solid curves in the Q_T distribution shows the prediction of the pure NLO $\mathcal{O}(\alpha_s)$ (fixed-order) calculation, without resummation, for the $q\bar{q}$ and qg subprocesses, excluding fragmentation. For Q_T

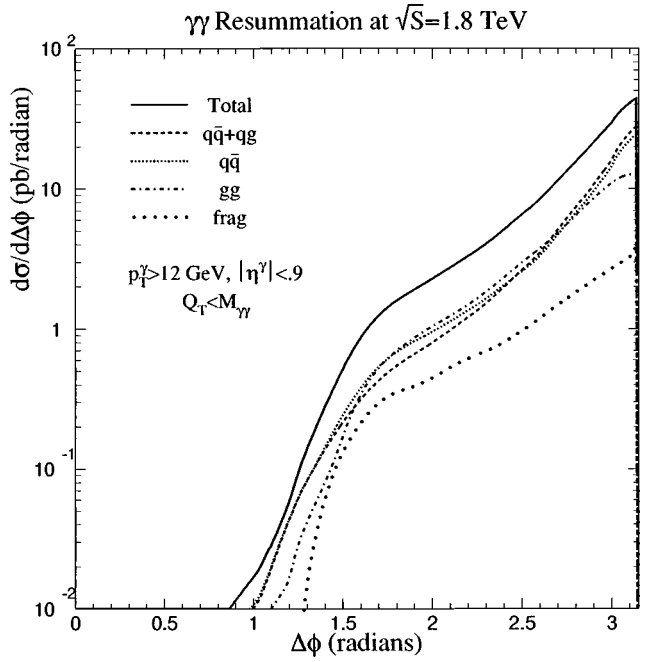

FIG. 11. The predicted distribution for the difference between the azimuthal angles of the photons $\Delta\phi_{\gamma\gamma}$ from the resummed calculation. The additional cut $Q_T < M_{\gamma\gamma}$ has been applied to reduce the theoretical uncertainty.

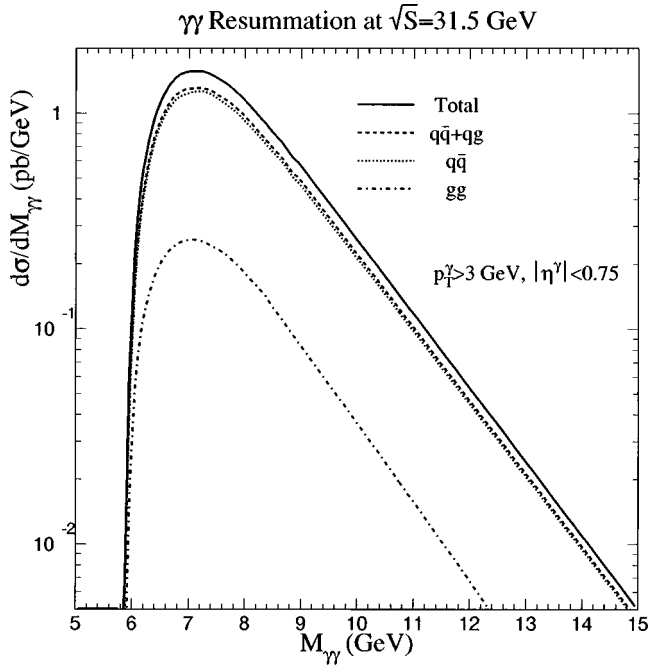

FIG. 12. The predicted distribution for the invariant mass of the photon pair $M_{\gamma\gamma}$ from the resummed calculation appropriate for $pN \to \gamma\gamma X$ at $\sqrt{S} = 31.5$ GeV.

$\gtrsim$25 GeV, the lower solid curve is very close to the long-dashed $(q\bar{q}+qg)$ curve obtained after resummation, as is expected. As Q_T decreases below $Q_T \simeq 25$ GeV, all-orders resummation produces significant changes. Most apparent, perhaps, is that the $Q_T \to 0$ divergence in the fixed-order calculation is removed. However, there is also a marked difference in shape over the interval $5 < Q_T < 25$ GeV between the fixed-order $q\bar{q}+qg$ result and its resummed counterpart. These are general features in a comparison of resummed and NLO calculations [6–14].

B. Fixed-target energy

The fixed-target experiment E706 [17] at Fermilab has collected diphoton data from the collision of a p beam on a Be ($A = 9.01$, $Z = 4$) target at $\sqrt{S} = 31.5$ GeV. The kinematic cuts applied to the resummed prediction in the center-of-mass frame of the beam and target are $p_T^\gamma > 3$ GeV and $|\eta^\gamma| < 0.75$. No photon isolation is required. The same phenomenological inputs are used for this calculation as for the calculation at collider energies. The Be nucleon target is treated as having an admixture of 4/9.01 proton and 5.01/9.01 neutron parton distribution functions. The A dependence effect appears to be small in the prompt photon data (the effect is parametrized as A^α and the measured dependence is $\alpha \simeq 1$), and so it is ignored [26].

Figures 12–14 show the same distributions discussed previously. Because of the kinematic cuts, the relative contribution of gluon initiated processes is highly suppressed, except at large Q_T, where the gg box contribution is seen to dominate, and at large $M_{\gamma\gamma}$, where the qg contribution is dominant. The fragmentation contribution (not shown) is minimal (of a few percent). The dominance of gg resummation over the $q\bar{q}$ resummation at large Q_T in Fig. 13 occurs because it

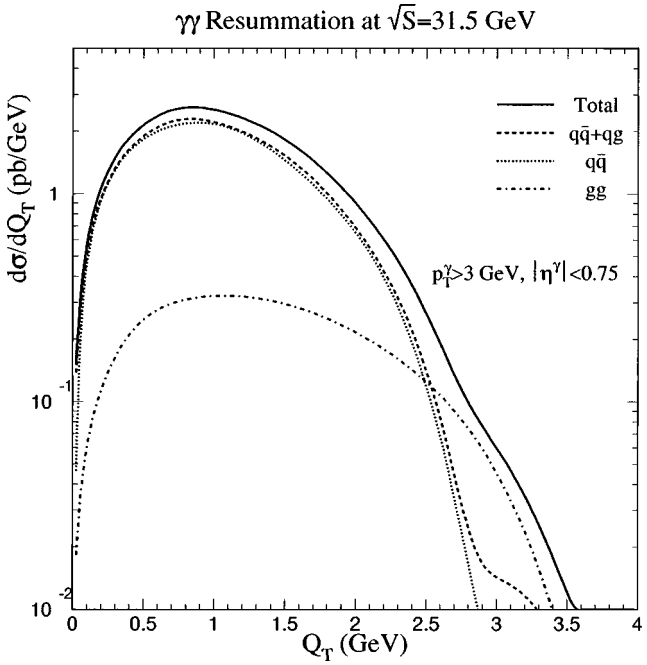

FIG. 13. The predicted distribution for the transverse momentum of the photon pair Q_T from the resummed calculation appropriate for $pN \rightarrow \gamma\gamma X$ at $\sqrt{S}=31.5$ GeV.

is more likely (enhanced by the ratio $C_A/C_F=9/4$) for a gluon to be radiated from a gluon than a quark line. The exact height of the distribution is sensitive to the form of the nonperturbative function (in the low Q_T region) and to the approximation made in calculating the NLO corrections [of $\mathcal{O}(\alpha_{em}^2\alpha_s^3)$] to the hard scattering. However, since $Q_T<Q$ is satisfied for the set of kinematic cuts, the final answer with complete NLO corrections should not differ significantly from the result reported here.

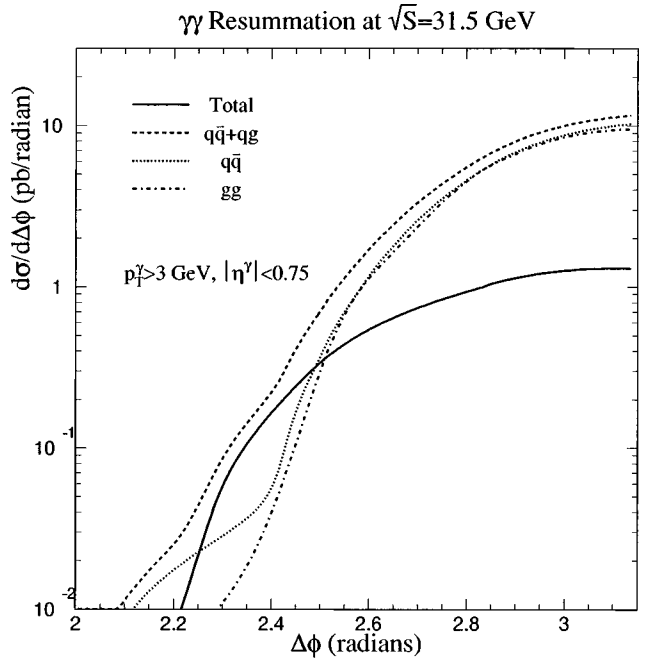

FIG. 14. The predicted distribution for the difference between the azimuthal angles of the photons $\Delta\phi_{\gamma\gamma}$ from the resummed calculation appropriate for $pN \rightarrow \gamma\gamma X$ at $\sqrt{S}=31.5$ GeV.

The scale dependence of the calculation was checked by comparing with the result obtained with $C_2=C_1/b_0=0.5$, $C_3=b_0$, and $C_4=1$. The $q\bar{q}$ rate is not sensitive to the scale choice, and the gg rate increases by less than about 20%. This insensitivity can be understood as follows. For the E706 data, the nonperturbative physics completely dominates the Q_T distribution. The perturbative Sudakov resummation is not important over the entire Q_T region, and the NLO Y piece is sizable only for $Q_T>3$ GeV where the event rate is small. Since the LO $q\bar{q}$ rate does depend on α_s, and the LO gg rate is proportional to $\alpha_s^2(C_2 M_{\gamma\gamma})$, the gg rate increases for a smaller C_2 value, but the $q\bar{q}$ rate remains about the same. In conclusion, the E706 data can be used to constrain the nonperturbative functions associated with the $q\bar{q}$ and gg hard processes in hadron collisions.

V. DISCUSSION AND CONCLUSIONS

Prompt photon pair production at fixed target and collider energies is of interest in its own right as a means of probing the dynamics of strong interactions. The process is of substantial interest also in searches for new phenomena, notably the Higgs boson.

In this paper, a calculation is presented of the production rate and kinematic distributions of photon pairs in hadronic collisions. This calculation incorporates the full content of the next-to-leading order contributions from the $q\bar{q}$ and qg initial-state subprocesses, supplemented by resummation of contributions to these subprocesses from initial state radiation of soft gluons to all orders in the strong coupling strength. The computation also includes important contributions from the gg box diagram. The gg contributions from initial-state multiple soft gluons are resummed to all orders, but the NLO contribution, of $\mathcal{O}(\alpha_{em}^2\alpha_s^3)$, to the hard scattering subprocess is handled in an approximate fashion. The approximation should be reliable at relatively small values of the pair transverse momentum Q_T as compared to the invariant mass of the photon pair $M_{\gamma\gamma}$. At collider energies, the gg contribution is comparable to that of the $q\bar{q}$ and qg contributions over a significant part of phase space where $M_{\gamma\gamma}$ is not large, and its inclusion is essential. The exact $\mathcal{O}(\alpha_{em}^2\alpha_s^3)$ corrections to the gg box diagram should be calculated to test the validity of the approximations made in this calculation. Finally, the calculation also includes long-distance fragmentation contributions at leading order from the subprocess $qg \rightarrow \gamma q$, followed by fragmentation of the final quark, $q \rightarrow \gamma X$. After photon isolation, fragmentation plays a relatively minor role. The fragmentation contribution is computed in two ways: first, in the standard parton model collinear approximation and, second, with a Monte Carlo shower simulation. This overall calculation is the most complete treatment to date of photon pair production in hadronic collisions. Resummation plays a very important role, particularly in the description of the behavior of the Q_T distribution at small to moderate values of this variable, where the cross section takes on its largest values.

The resummed calculation is necessary for a reliable prediction of kinematic distributions that depend on correlations between the photons. It is a significant improvement over fixed-order NLO calculations that do not include the effects

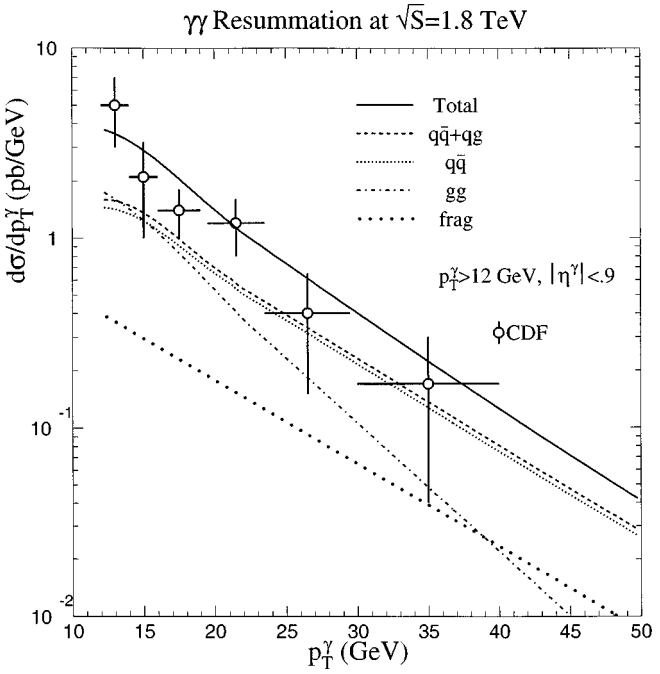

FIG. 15. The predicted distribution for the photon transverse momentum from the resummed calculation compared to the CDF data.

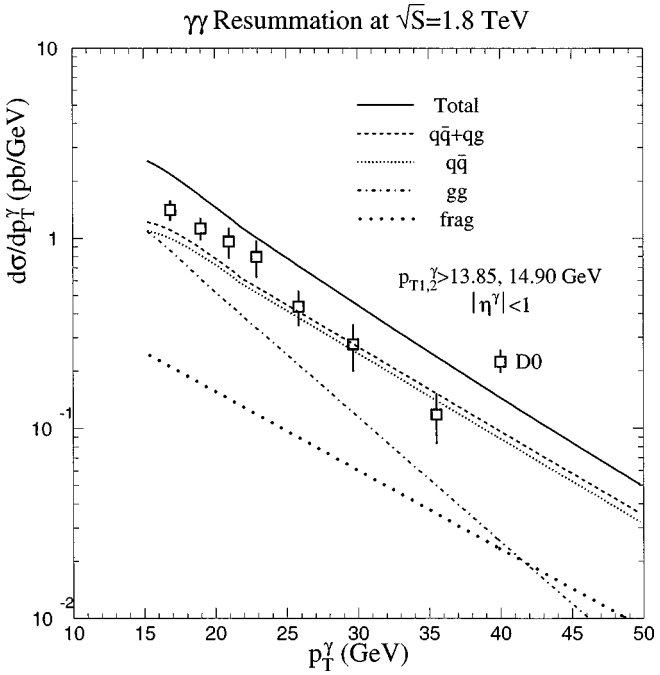

FIG. 16. The predicted distribution for the photon transverse momentum from the resummed calculation compared to the DØ data.

of initial-state multiple soft-gluon radiation. Furthermore, even though the hard scattering $q\bar{q}$ and qg subprocesses are computed to the same order in the resummed and fixed-order NLO calculations, the cross sections from the two calculations can differ after kinematic cuts are imposed [10].

The results of the calculation are compared with data from the CDF and DØ Collaborations, and the agreement is generally good in both absolute normalization and shapes of the distributions in the invariant mass $M_{\gamma\gamma}$ of the diphoton system, the pair transverse momentum Q_T, and the difference in the azimuthal angles $\Delta\phi$. Discrepancies with CDF results at the smallest values of Q_T and $\Delta\phi$ near π might originate from the strong dependence on the nonperturbative functions in this kinematic region. In comparison with the DØ data, there is also evidence for disagreement at intermediate and small values of $\Delta\phi$. The region of intermediate $\Delta\phi$, where the two photons are not in a back-to-back configuration, is one in which the full treatment of three-body final-state contributions of the type $\gamma\gamma j$ are important, with $j=q$ or g. The distributions in Figs. 5 and 8 suggest that an exact calculation of the NLO contribution associated with the gg initial channel would ameliorate the situation and will be necessary to describe data at future high energy hadron colliders.

Predictions are also presented in the paper for $pN \rightarrow \gamma\gamma X$ at the center-of-mass energy 31.5 GeV, appropriate for the E706 fixed-target experiment at Fermilab. The large Q_T and small $\Delta\phi$ behavior of the kinematic distributions is dominated by the resummation of the gg initial state. Nonperturbative physics controls the Q_T distribution, and neither the perturbative Sudakov nor the regular NLO contribution plays an important role, except in the very large Q_T region where the event rate is small. For the E706 kinematics, the requirement $Q_T < Q$ is generally satisfied. Therefore, the approximate gg calculation presented in this work should be reliable.

In this calculation, the incident partons are assumed to be collinear with the incident hadrons. A recurring question in the literature is the extent to which finite ''intrinsic'' k_T may be required for a quantitative description of data [27,17]. An important related issue is the proper theoretical specification of the intrinsic component [28]. In the CSS resummation formalism, this physics is included by properly parametrizing the nonperturbative function $\tilde{W}^{NP}(b)$, which can be measured in Drell-Yan, W, and Z production. Because photons participate directly in the hard scattering, because their momenta can be measured with greater precision than that of hadronic jets or heavy quarks, and because the $\gamma\gamma$ final state is a color singlet, the reaction $p\bar{p} \rightarrow \gamma\gamma X$ may serve as a particularly attractive laboratory for the understanding of the role of intrinsic transverse momentum. The agreement with data on the Q_T distributions in Figs. 4 and 7 is suggestive that the CSS formalism is adequate. However, the separate roles of gluon resummation and the assumed nonperturbative function in the successful description of the Q_T distributions are not disentangled. In the non-perturbative function of Eq. (12), the dependence on b (and, thus, the behavior of $d\sigma/dQ_T$ at small Q_T) is predicted to change with both Q and the values of the parton momentum fractions x_i. At fixed Q, dependence on the values of the x_i translates into dependence on the overall center-of-mass energy of the reaction. As data with greater statistics become available, it should be possible to verify these expectations. In combination with similar studies with data on massive lepton-pair production (the Drell-Yan process), it will be possible to determine whether the same non-perturbative function is applicable in the two cases, as is assumed in this paper.

The diphoton data may allow a study of the nonperturba-

tive as well as the perturbative physics associated with multiple gluon radiation from the *gluon*-initiated hard processes, which cannot be accessed from Drell-Yan, $W^{\pm}$, and Z data. With this knowledge, it may be possible to improve calculations of single photon production and other reactions sensitive to gluon-initiated subprocesses. In the DØ data analysis [16], an asymmetric cut is applied on the transverse momenta (p_T^{γ}) of the two photons in the diphoton event. This cut reduces the effect of multiple gluon radiation in the event. To make the best use of the data for probing the interesting multiple gluon dynamics predicted by the QCD theory, a symmetric p_T^{γ} cut should be applied.

Note added in proof. Data are also available on the transverse momentum distribution $d\sigma/dp_T$ of individual photons produced in diphoton events, $p+\bar{p}\rightarrow\gamma+\gamma+X$. Our expectations for the CDF cuts and a comparison with the CDF data [15] are shown in Fig. 15, and our expectations for the DØ cuts and comparison with their data [16] are shown in Fig. 16. The qualitative features present in Figs. 3–5 and 6–8 are also evident in these two plots. The theoretical predictions are in good agreement with both the shape and normalization of the CDF data and with the shape of the DØ distribution. The normalization of the DØ data appears low.

ACKNOWLEDGMENTS

We thank J. Huston for explaining the Tevatron and fixed-target data. Also, C.-P.Y. and C.B. thank the CTEQ Collaboration and C. Schmidt for many invaluable discussions, and S.M. thanks R. Blair, S. Kuhlmann, J. Womersley, L. Gordon, and C. Coriano for useful conversations. This work was supported in part by the NSF under grant PHY-9507683 and the U.S. Department of Energy under grant W-31-109-ENG-38.

[1] P. Aurenche, A. Douiri, R. Baier, M. Fontannaz, and D. Schiff, Z. Phys. C **29**, 459 (1985).
[2] E. L. Berger, E. Braaten, and R. D. Field, Nucl. Phys. **B239**, 52 (1984).
[3] B. Bailey, J. F. Owens, and J. Ohnemus, Phys. Rev. D **46**, 2018 (1992).
[4] G. Sterman, Nucl. Phys. **B281**, 310 (1987); S. Catani and L. Trentadue, *ibid.* **B327**, 323 (1989); **B353**, 183 (1991); S. Catani, G. Turnock, B. R. Webber, and L. Trentadue, Phys. Lett. B **263**, 491 (1991); Nucl. Phys. **B407**, 3 (1993).
[5] E. Laenen, J. Smith, and W. L. van Neerven, Nucl. Phys. **B369**, 543 (1992); E. L. Berger and H. Contopanagos, Phys. Rev. D **54**, 3085 (1996); S. Catani, M. L. Mangano, P. Nason, and L. Trentadue, Nucl. Phys. **B478**, 273 (1996).
[6] G. Altarelli, R. K. Ellis, M. Greco, and G. Martinelli, Nucl. Phys. **B246**, 12 (1984).
[7] J. Collins and D. Soper, Nucl. Phys. **B193**, 381 (1981); **B213**, 545(E) (1983); **B197**, 446 (1982); J. Collins, D. Soper, and G. Sterman, *ibid.* **B250**, 199 (1985).
[8] J. Kodaira and L. Trentadue, Phys. Lett. **112B**, 66 (1982); **123B**, 335 (1982); P. B. Arnold and R. P. Kauffman, Nucl. Phys. **B349**, 381 (1991); R. K. Ellis, D. A. Ross, and S. Veseli, *ibid.* **B503**, 309 (1997).
[9] C. T. H. Davies, W. J. Stirling, and B. R. Webber, Nucl. Phys. **B256**, 413 (1985).
[10] C. Balázs, J. W. Qiu, and C.-P. Yuan, Phys. Lett. B **355**, 548 (1995); C. Balázs and C.-P. Yuan, Phys. Rev. D **56**, 5558 (1997).
[11] S. Catani, E. D'Emilio, and L. Trentadue, Phys. Lett. B **211**, 335 (1988); I. Hinchliffe and S. F. Novaes, Phys. Rev. D **38**, 3475 (1988); R. P. Kauffman, *ibid.* **44**, 1415 (1991).
[12] C.-P. Yuan, Phys. Lett. B **283**, 395 (1992).
[13] E. L. Berger and R.- B. Meng, Phys. Rev. D **49**, 3248 (1994).
[14] P. Chiappetta, R. Fergani, and J. Ph. Guillet, Phys. Lett. B **348**, 646 (1995).
[15] L. Nodulman, in *ICHEP '96*, Proceedings of the 28th International Conference on High Energy Physics, Warsaw, Poland, edited by Z. Ajduk and A. K. Wroblewski (World Scientific, Singapore, 1997), p. 1064.
[16] DØ Collaboration, Pierrick Hanlet, in *Proceedings of the International Euroconference on Quantum Chromodynamics (QCD97)*, Montpellier, France, 1997 [Nucl. Phys. B (Proc. Suppl.) (in press)].
[17] Fermilab E706 Collaboration, L. Apanasevich *et al.*, , ''Evidence for Parton k_T Effects in High-p_T Particle Production,'' Report No. FERMILAB-PUB-97/351-E, hep-ex/9711017; M. Zielinski *et al.*, in *Proceedings of the International Euroconference on Quantum Chromodynamics (QCD97)* [16].
[18] J. Collins and D. Soper, Phys. Rev. D **16**, 2219 (1977).
[19] Yu. L. Dokshitzer, Sov. Phys. JETP **46**, 641 (1977); V. N. Gribov and L. N. Lipatov, Sov. J. Nucl. Phys. **15**, 78 (1972); G. Altarelli and G. Parisi, Nucl. Phys. **B126**, 298 (1977).
[20] G. A. Ladinsky and C.-P. Yuan, Phys. Rev. D **50**, 4239 (1994).
[21] S. Catani and M. H. Seymour, Nucl. Phys. **B485**, 291 (1997).
[22] E. L. Berger, X. Guo, and J. Qiu, Phys. Rev. D **54**, 5470 (1996).
[23] T. Sjöstrand, Comput. Phys. Commun. **82**, 74 (1994).
[24] H. L. Lai, J. Huston, S. Kuhlmann, F. Olness, J. Owens, D. Soper, W. K. Tung, and H. Weerts, Phys. Rev. D **55**, 1280 (1997).
[25] Wei Chen, DØ diphoton data, http://www-d0.fnal.gov/ wchen/ Welcome.html, and private discussion.
[26] L. Sorrell, Ph.D. thesis, Michigan State University, 1994.
[27] E. L. Berger, J. Donohue, and S. Wolfram, Phys. Rev. D **17**, 858 (1978), and references therein; E. L. Berger, in *Proceedings of the Workshop on Physics at Fermilab in the 1990's*, Breckenridge, CO, 1989, edited by D. Green and H. Lubatti (World Scientific, Singapore, 1990), pp. 64–102; J. Huston, E. Kovacs, S. Kuhlmann, H. L. Lai, J. F. Owens, and W. K. Tung, Phys. Rev. D **51**, 6139 (1995); H. Baer and M. H. Reno, *ibid.* **54**, 2017 (1996).
[28] W. E. Caswell, R. R. Horgan, and S. J. Brodsky, Phys. Rev. D **18**, 2415 (1978); S. J. Brodsky and C.-R. Ji, *ibid.* **33**, 2653 (1986).